# Inactivation of Airborne Microorganisms using Dielectric Barrier Discharge Technology

Jaione Romero-Mangado[1], Felipe Soberon[2], Sami Sainio[3], Dennis Nordlund[4], Ian T. Saunders[1], Gurusharan Singh[5], Graham Deane[2], Kevin Maughan[2], Stephen Daniels[5], David Loftus[1], M. Meyyappan[1], Jessica Koehne[1], Ram P. Gandhiraman[1*]

[1]NASA Ames Research Center, Moffett Field, CA-94035, USA

[2] Novaerus Inc. 111 N. Canal St. Suite 165, Chicago, IL 60606, USA

[3] Department of Electrical Engineering and Automation, School of Electrical Engineering, Aalto University, 02150, Espoo, Finland

[4]Stanford Synchrotron Radiation Lightsource, Stanford Linear Accelerator Center, Menlo Park, CA 94025, USA

[5]National Center for Plasma Science and Technology, Dublin City University, Dublin-9, Ireland

## Abstract

The primary goal of this work is to study the efficacy of dielectric barrier discharge (DBD) technology for deactivating airborne micro-organisms. E. coli nebulised in air was exposed to the DBD and the bacterial sample collected from air was analyzed in detail. Reculturing of the collected bacteria showed deactivation of E. coli. In order to understand the mechanisms of bacterial deactivation, the bacterial samples collected from air in the vicinity of the DBD were analysed for surface chemical change and morphological change upon DBD treatment. Scanning electron microscopy imaging of the E. coli shows that the bacteria undergoes physical distortion to varying degrees from formation of pores to severe structural distortion. Fourier transform infrared spectroscopy analysis showed that the bacteria underwent severe oxidation resulting in

formation of hydroxyl groups and carbonyl groups and a significant reduction of amine functionalities and phosphate groups. High resolution N1s core level photoemission spectroscopic measurements confirmed the presence of oxide peak and a decrease in the peak intensity of the protonated amine compared to untreated E.coli suggest oxidation of the outer layer of the cell wall.

*Corresponding author email: ramprasad.gandhiraman@nasa.gov Ph: +1 650 604 4702

Key words: air decontamination, E. coli, sterilization, dielectric barrier discharge, plasma

## Introduction

Nosocomial infections have become a worldwide public health concern, resulting in prolonged hospitalisation of patients, increased human suffering and spiraling healthcare costs. Recent estimates place the annual cost of nosocomial infections at over $45 billion every year to the U.S. healthcare system alone.[1] Decontamination of air is an important area of research with significant impact on several environments including hospitals, long duration space flights and other enclosed areas that are prone for microbial contamination.[2] Ross et. al. analyzed air samples from the homes of 44 asthmatic individuals and concluded that increased concentrations of gram negative bacteria present in the air increased the severity of asthma.[3] The most commonly used technologies for air cleaning include high efficiency particulate air filters, UV irradiation, chemicals (spray, gel), steam (autoclave), and gas spray (ozone, hydrogen peroxide).[4-11] These methods, while popular, often provide sub-optimal outcomes such as creating bacterial resistance, developing mutagenic outcomes if bacteria are under-exposed and are responsible for numerous health hazards when operated incorrectly (for example, radiation exposure in the case of UV). Prolonged exposure to radiation could cause skin irritation in operators, patients and staff.[12,13]

Air filters depend on the mechanical filtration of airborne particles and their drawback is that the contaminated air has to pass through the filter, trapping clusters of bacteria but consequently causing a localized bio-hazard for the maintenance staff. Standard HEPA filtration may also allow individual bacteria to pass through its porous surface once the original clusters have desiccated, and is unable to arrest the transit of smaller pathogenic organisms such as viruses. Another problem with traditional air filtration is that there is a significant drop in air pressure across the filter medium, increasing the cost of continuous operation over their life cycle and

requiring filter replacement on a frequent basis. UV irradiation for air disinfection comes in several forms, including full intensity irradiation of room with no occupants in it and shielded UV irradiation which is done with no restriction to human occupation.[14] One of the biggest drawbacks of UV irradiation is that it requires direct 'line of sight' exposure for it to be effective, and 'shadowing' may occur when used to treat airborne bacteria, a process whereby the exposed upper layers of a bacterial cluster are deactivated while providing a protective shield for the bacteria below them, particularly those that form biofilms.[15] While the above technologies are often used on their own, they may be combined; for example, a combination of high efficiency particulate air filters with UV irradiation was shown to be effective in reducing 60% of the bio-aerosols in a contaminated room.[16] Pal et. al., reported titanium dioxide nanoparticle mediated photocatalytic inactivation of airborne E. coli in a continuous flow reactor,[17,18] and fluorescent light inactivation of gram negative and gram positive bacteria.[19] Kowalski et. al. reported killing E.coli in 10-480 seconds using high concentrations of ozone (300-631 ppm).[20]

In recent years, cold atmospheric pressure plasmas have gained significant recognition in the field of healthcare, for example in the treatment of living cells, sterilization, wound healing and blood coagulation[21]. The plasmas are nontoxic, provide rapid and continuous anti-bacterial treatment, leave no residues to clean up and are easy to scale up, compared to other approaches. **T**he dielectric barrier discharge (DBD) based air decontamination method requires the air and biomolecules to pass in close proximity to the discharge source and several synergistic decontamination mechanisms are believed to increase the overall decontamination efficacy[22-25]. Here, we present a DBD based air decontamination technology using a novel electrode for generating the discharge. The study aims to explore the efficacy of DBD technology for deactivating airborne micro-organisms and assess the effects of the atmospheric pressure plasma

specifically on E. coli micro-organisms. In order to understand the mechanisms of bacterial deactivation it is necessary to examine the bacterial surface chemical and topographical change upon plasma treatment. Topographical features have been observed here using scanning electron microscopy (SEM). Understanding the relation of surface chemical change to cell death is crucial and therefore, a detailed analysis of the chemical changes to the proteins, lypopolysaccharides and the outer cell wall of the E. coli upon exposure to DBD has been carried out using fourier transform infrared spectroscopy (FTIR) and x ray photoelectron spectroscopy (XPS).

E. coli bacteria was chosen as a representative organism for this study because of its prevalence in many human occupied spaces, its rod-like structure makes it easier to see morphological surface changes and its propensity to cause infectious diseases; including wound infections, neonatal meningitis, inflammation of abdominal wall, bacteria and pneumonia.

**Methods**

Materials:

*Escherichia coli* (Migula) Castellani and Chalmers (ATCC 25922) was rehydrated in 1 ml of Tryptic soy Broth (BD 211825). The aliquot was aseptically transferred into a tube containing 5 ml of Tryptic Soy Broth and incubated overnight with shaking at 37℃. The bacterial suspension was then centrifuged at 1000 rpm for 10 minutes, the supernatant was discarded and the cells were washed down four times with distilled water. The cell culture was transferred to a tube and vortexed to re-suspend the bacterial cell pellet in distilled water.

Experimental Setup:

A commercially available plasma based air decontamination system (NV200, Novaerus Inc.) was used. The DBD electrode consists of two coaxial cylindrical mesh coils (304 stainless steel, 0.2 mm diameter wire) separated by a dielectric, borosilicate glass tube (Fig. 1). The glass tube has the following dimensions: 80 mm length, 22.5 mm internal diameter, and 28 mm outer diameter. A high alternating voltage, 4 kV, is applied to the coils via a step-up transformer. A fan inside the NV200 unit is used to draw the air containing bioaerosol into the unit. The DBD tool was placed inside a Bio-Safety Cabinet (Nuaire, Class II, Type A2, Model NU-425-400) and a compressor nebulizer (OMROM Compressor nebulizer model NE-C29-E) was attached to the input of the system in order to aerosolize the bacterial particles for testing. All vents located on the system were sealed and a platform was placed over the top of the system to ensure the aerosolized particles had a direct route through the system. The bacterial suspension containing *E.coli* and distilled water of quantity 1 ml was transferred to the OMROM compressor nebulizer. The aerosolized particles were fed through the input and any viable particles were collected at the output in Tryptic Soy Agar plates (BD 236950). The agar plates were left in front of the output of the DBD NV200 tool and were replaced every minute for 5 minutes. The agar plates were incubated overnight at 37℃ and after the incubation, colony forming units were observed on the plates as shown in figure 2a. In another set of experiment, the agar plates were placed continuously for 1 to 5 minutes and the colony forming unit counts upon reculture is shown in figure 2b. Two different sized petri dishes 100 mm diameter and 60 mm diameter were used. For the experiment in Figure 2a, 100 mm diameter petri dishes were used with both the fan and electrodes turned ON and OFF simultaneously. For the experiment in Figure 2b, 60 mm diameter petri dishes were used with plasma ON and OFF, while having the fan ON for both the cases. There is no scientific reason for the use of different sized petri dishes. The concentration of E.

coli in each plate was calculated using the following formula: bacteria/ml= number of colonies x dilution of sample.

Characterization:

For SEM imaging, bacterial cells on silicon wafer were fixed in a solution of 2.5% Glutaraldehyde (Sigma-Aldrich) in Phosphate Buffered Saline (ATCC) for 2 hours and as a second fixative procedure, in a 2% Osmium Tetroxide (Ted Pella, Inc.) in PBS for 1.5 hours. The samples were then dehydrated in gradually increasing concentrations of ethanol from 60% to 100% in deionized water and chemically dried using Hexamethyldisilazane (Sigma-Aldrich) for 5 minutes. In order to preserve the samples from reacting with water from humidity, they were placed in a vacuum desiccator overnight. SEM imaging was performed using S4800 scanning electron microscope (Hitachi, Pleasanton, CA).

FTIR measurements were carried out using a Perkin Elmer Spectrum GX system. As the transmission mode measurement was carried out, single side polished silicon wafers were used as substrates. An untreated silicon substrate was used as a background substrate for the measurement. Each measurement was an average of 200 scans.

The N1s core level x ray photo emission spectroscopy (XPS) measurements were performed on beamline 10-1 (bending magnet endstation, spherical grating monochromator) at the Stanford Synchrotron Radiation Lightsource (SSRL).[26] A gold grid in the beam path upstream of the chamber was used for normalization of the incoming flux. The samples were mounted on an aluminum stick with carbon tape and all the measurements were done under UHV conditions (< $1x10^{-8}$ torr) in a generic XPS chamber. Peak fitting was performed using Casa XPS using Shirley background and Gaussian-Lorentzian distribution. For XPS measurements, the bacterial samples

collected on silicon wafer were freeze dried using Labconco's FreeZone 4.5 Liter Freeze Dry Systems.

**Results**

Figure 1 shows the (a) Schematic of the NV200 DBD system, (b) diagram of the assembled coil, (c) cross section illustrating the air flow around the dielectric barrier discharge, (d) the coil parts, and (e) the experimental setup for airborne inactivation of E. coli and sample collection. The bio-aerosol containing nebulized E. coli was directed at the top of the DBD tool which has an internal fan that sucks the contaminated air towards the DBD placed inside the tool. The decontaminated air passes out of the bottom outlet. The deactivated bacteria was collected near the bottom outlet in a silicon wafer and agar plates for characterization and re-culturing respectively. The purpose of a partial shield between the nebulizer and the bottom outlet in the DBD tool is to prevent direct settlement of bacteria on to the silicon wafer and the culture plate. The DBD design shown in Figure 1 (right) contains metal electrodes separated by a dielectric.

Figure 2 shows the reduction numbers of nebulized e.coli exposed to DBD. E.coli exposed to DBD was collected, re-cultured and counted. Comparison of the e.coli counts with samples collected in DBD OFF state shows a clear reduction of air borne e.coli exposed to DBD. Figure 2 shows two plots (Left) both fan and electrode were either ON and OFF together and (Right) fan was ON throughout the experiment and the electrode was turned ON and OFF independently. In both the cases, the DBD ON results in deactivation of the airborne E. coli. The difference in the E. coli counts between the left and right is due to the difference in the surface area made available for collection of the air borne microbes i.e. the difference in petri dish size between the experiments.

Figure 3 shows a photograph of captured E. coli in DBD OFF and DBD ON states displaying the deactivation of air borne E. coli. Figure 4 shows SEM images of the samples at various stages. The nebulized E. coli was exposed to DBD and collected from air on a silicon wafer. Upon fixing of the microbes using the procedure described in the experimental section earlier, SEM imaging was carried out on several sets of samples to study the effect of DBD on the airborne bacteria. Untreated E. coli is smooth with intact surface and the DBD-treated bacteria are rough with holes. The DBD alters the topographical features of E. coli to a significant extent ranging from formation of big holes to severe structural deformation resulting in cell death. Physical distortion to the bacterial cell wall happens to varying degrees. It is hypothesized that the degree of distortion depends on the proximity of the bacteria to the electric field and the plasma discharge source. Formation of holes and structural deformation of sterilized e-coli similar to our observation has been reported by others using techniques such as biocide emusions[27] and photocatalysis.[28]

The FTIR data for the untreated and DBD-treated E.coli are shown in figure 5. The peak attributions are made based on the vast FTIR spectroscopy literature on intact and damaged bacterial cells.[29-34]The broad asymmetric absorption peak between 3000 and 3500 $cm^{-1}$ comprises of multiple bands. Though the peaks were not distinctly resolved, the asymmetric peak shape indicates multiple components. The characteristic peaks at 3305 and 3066 $cm^{-1}$ are assigned to amide I and amide II, respectively. A shoulder peak observed around 1730 $cm^{-1}$ corresponds to C=O stretching vibrations of ester functional groups probably from the lipids and fatty acids. The vibration bands centered around 1653 $cm^{-1}$ and 1550 $cm^{-1}$ correspond to amide vibrations associated with proteins. The amide I band centered around 1653 $cm^{-1}$ can be resolved into three separate peaks at 1636 $cm^{-1}$, 1655 $cm^{-1}$ and 1687 $cm^{-1}$. The 1655 $cm^{-1}$ peak is

attributed to C=O stretching vibration of amides in the α helical content of the protein, 1636 $cm^{-1}$ correspond to β sheets and 1687 $cm^{-1}$ is related to antiparallel β sheets and aggregated strands.[35-37] The amide II band centered around 1550 $cm^{-1}$ band is attributed to N-H deformation of amides associated with proteins including contributions from the C-N stretching vibrations of the peptide group. The absorption peaks between 2800 and 3000 $cm^{-1}$ correspond to the stretching vibrations of alkyl groups ($CH_2$ and $CH_3$) present in the bacterial cell wall fatty acids. The peaks at 2960 $cm^{-1}$ and 2923 $cm^{-1}$ correspond to asymmetric stretching vibration of $CH_3$ and $CH_2$ and 2870 $cm^{-1}$ and 2851 $cm^{-1}$ correspond to symmetric stretching vibration of $CH_3$ and $CH_2$ respectively. The peaks at 1460 and 1394 $cm^{-1}$ correspond to $CH_3$ and $CH_2$ asymmetric and symmetric deformation of proteins. The presence of a band at 1402 $cm^{-1}$ has been attributed to the C-O stretching vibration of carboxylic groups.[38] The peak at 1240 $cm^{-1}$ is due to the P=O asymmetric stretching mode of the phospholipid phosphodiester backbone of nucleic acids DNA and RNA.[39] The region between 1000 and 1100 $cm^{-1}$ with peaks centered around 1040 and 1100 $cm^{-1}$ has multiple components corresponding to the C-O-C and C-O-P stretching of diverse polysaccharides groups and P=O symmetric stretching overlapping with the vibrations of the sugar rings of lipopolysaccharides. The peak at 1033 $cm^{-1}$ is attributed to C-OH of phosphorylated proteins and associated alcohols. We are not certain about the new intense peak centered around 1850 $cm^{-1}$ in the DBD treated E. coli. The carbonyl C=O stretching vibrations of esters and carboxylic groups from lipids and fatty acids, in general, appear around 1740 $cm^{-1}$. As we did not find any literature for attributing the 1850 and 1975 $cm^{-1}$ vibrational bands, these peaks are left unassigned. Appearance of a new band around 930 $cm^{-1}$ in the DBD treated E. coli is due to the formation of OH species caused by oxidation. An adjacent peak around 956 $cm^{-1}$ is attributed to asymmetric stretching vibration of O-P-O functionalities.

Figure 6 shows the N1s core level x ray photoemission spectrum (high resolution scan) of untreated and DBD treated E. coli. The N1s peak of untreated E. coli can be resolved in to two components and that of DBD treated E. coli can be resolved in to three components. The major peak at 399.8 eV is due to non-protonated nitrogen as in amines and amides. The low intensity peak at 401.4 eV is due to protonated amines which are likely from the basic amino acid sequence.[40-43]

**Discussion**

DBD based inactivation of the air borne E. coli as observed in figures 2 and 3 can be caused by multiple factors. The possible contributions arising from topographical and chemical changes are discussed in detail below. The gram negative bacteria contain cytoplasmic membrane, peptidoglycan layer and outer membrane. The ability of the cell to withstand high internal osmotic pressure and the maintenance of the cell shape is due to peptidoglycan layer that consists of amino sugars and amino acids.[44,45] The outer membrane contains structural proteins, receptor molecules and phospholipids and acts as a selective permeability barrier containing hydrophilic diffusion channels.[46-49] It has been reported that the change in permeability of the membrane during the inactivation process results in leakage of Potassium ion (K+), a vital component involved in protein synthesis and essential for cell viability.[50,51] Formation of pores, as observed in the SEM images, is more likely to have caused potassium ion leak resulting in cell death. The structural deformation suggests extensive chemical degradation of the microbe through the action of the charged species generated by DBD.

The role of hydroxyl radicals and reactive oxygen species in E.coli inactivation has been studied by several research groups.[52,53] The extents of this molecular damage were assessed using

infrared spectroscopy by observing the major chemical components such as C=O and N-H vibrations of amides associated with proteins, C=O vibrations of esters from lipids, CH vibrations of the bacterial cell walls, P=O vibrations of the phosphodiester of nucleic acids and the C-O-C vibrations of polysaccharides.[29] The formation of free and hydrogen bonded hydroxyl groups in the decontaminated E.coli has been observed here.

Exposure of the nebulized bacteria in air to DBD resulted in a significant change in chemical structure. Significant reduction in the intensity of broad stretching vibrations of amine between 3000 to 3500cm$^{-1}$ and the formation of hydrogen bonded and free hydroxyl groups between 3500 to 4000 cm$^{-1}$ is very evident. A broad shoulder peak centered around 3850 cm$^{-1}$ and an intense peak centered around 3665 cm$^{-1}$ correspond to O-H functionalities. The C=O stretching vibration and N-H deformation of amides associated with proteins in the range of 1655 and 1550 cm$^{-1}$ show a very clear variation. An enormous increase in the intensity of the peak centered around 1100 cm$^{-1}$ could be attributed to oxidation of P=O, C-O-C and C-O-P groups of lipopolysaccharides and other structural proteins and receptor molecules present in the outer layer. In the DBD treated E. coli, appearance of a new band caused by oxidation has been observed at around 930 cm$^{-1}$ due to the OH species and an adjacent peak around 956 cm$^{-1}$ attributed to asymmetric stretching vibration of O-P-O functionalities. All these observations suggest damage to the outer leaflet of the E. coli due to the exposure to DBD.

In both the untreated and DBD treated E. coli, the N1s core level photoemission spectra confirms the presence of non-protonated nitrogen as in amines and amides and protonated amines which are likely from the basic amino acid sequence. For the DBD-treated E. coli, an additional peak at 402.8 eV corresponding to oxidized species is prominent. Also, the peak intensity corresponding to the protonated amine in DBD-treated E. coli is decreased compared to that in untreated E. coli.

As the probing depth for XPS measurement is about 10 nm, the confirmation of oxide peak in the N1s high resolution scan and a decrease in the peak intensity of the protonated amine suggest oxidation of the outer layer of the cell wall.

The inactivation mechanism of the reactive oxygen species is based on its effect on cell membrane and intra cellular substances. As hydroxyl groups are permeable to cell membrane, the hydroxyl species penetrate the E. coli cell membrane, react with cytoplasmic substances and cause chromosomal DNA damage resulting in the deactivation[54]. This effect is clearly observed in figure 5 with the disappearance of one of the amide related peaks and an intense carbonyl peak formation.

**Conclusion**

The efficacy of DBD technology for decontamination of air borne microorganisms was tested and proved positive. The DBD technology is rapid and the inactivation occurs immediately upon an organism transporting through or making contact with the electric field and/or any radicals generated by DBD. The short time needed for inactivation of bacterial cells increases the usefulness of the plasma in everyday settings such as hospital and workplace environments. The effect of DBD on the morphology and surface chemistry of E. coli was studied in order to understand the underlying mechanism in the decontamination process. The electromagnetic field around the DBD coil causes severe distortion of the morphology of E. coli to varying degrees from formation of pores to shrinking and elongation of the cell structure possibly resulting in leakage of potassium ion. The oxidation and destruction components of protein, DNA and lipopolysaccharides present in the outer leaflet of the cell wall are evident from the FTIR spectroscopy and XPS.

**Acknowledgement**

Dr. R.P. Gandhiraman is with Universities Space Research Association subcontracted to NASA Ames Research Center under NASA cooperative agreement. Use of the Stanford Synchrotron Radiation Lightsource, SLAC National Accelerator Laboratory, is supported by the U.S. Department of Energy, Office of Science, Office of Basic Energy Sciences under Contract No. DE-AC02-76SF00515. The SSRL Structural Molecular Biology Program is supported by the DOE Office of Biological and Environmental Research, and by the National Institutes of Health, National Institute of General Medical Sciences (including P41GM103393). The contents of this publication are solely the responsibility of the authors and do not necessarily represent the official views of NIGMS or NIH.

**Conflict of interest statement**

None declared

**Funding source**

**Part of this research is funded by Novaerus Inc**

**References**

1. R D Scott II, Centers for Disease Control and Prevention, The Direct Cost of Healthcare-Associated Infections in U.S. Hospitals and the Benefits of Prevention, 2009

2. W.R. Jarvis. Selected aspects of the socioeconomic impact of nosocomial infections: morbidity, mortality, cost, and prevention. *Infect Control Hosp Epidemiol* 1996; **17**(8): 552-7.

3. M.A. Ross, L. Curtis, P.A. Scheff *et al*. Association of asthma symptoms and severity with indoor bioaerosols. *Allergy* 2000; **55**(8):705-11.

4. Philip E. Hockberger. A History of Ultraviolet Photobiology for Humans, Animals and Microorganisms. *J. Photochem. Photobiol.* 2002; **76**(6): 561–579

5. A. Davies, T. Pottage, A. Bennett, J. Walker. Gaseous and air decontamination technologies for Clostridium difficile in the healthcare environment. *J. Hosp. Infect.* 2011; **77(3)**: 199-203

6. A. E. Humphrey. Air Sterilization. *Adv. Appl. Microbiol.* 1960; **2**: 301–311

7. S. Aiba and A. Yamamoto. Distribution of bacterial cells within fibrous air sterilization filters. *J Biochem Microbiol.* 1959; **1 (2)**: 129–141

8. S. Roy, J. Gendron, M.-C. Delhoménie, L. Bibeau, M. Heitz, R. Brzezinski. Pseudomonas putida as the dominant toluene-degrading bacterial species during air decontamination by biofiltration. *Appl. Microbiol. Biotechnol.* 2003; **61 (4)**: 366-373

10. Y. Paz. Application of $TiO_2$ photocatalysis for air treatment: Patents' overview. *Appl. Catal., B* 2010; **99 (3–4)**: 448–460

11. J. Peral, X. Domènech, D. F. Ollis. Heterogeneous Photocatalysis for Purification, Decontamination and Deodorization of Air. *J. Chem. Technol. Biotechnol.* 1997; **70(2):**117–140.

12. E. Bermudez, J. B. Mangum, Wong B A, et al. Pulmonary responses of mice, rats, and hamsters to subchronic inhalation of ultrafine titanium dioxide particles. *Toxicol Sci,* 2004; **77**: 347—357

13. S. H. Sharma. Nanoneuroscience: Emerging concepts onnanoneuro toxicity and nanoneuroprotection. *Nanomed.* 2007; **2**: 753 —758

14. E. Levetin, R. Shaughnessy, C.A. Rogers, R. Scheir. Effectiveness of germicidal UV radiation for reducing fungal contamination within air-handling units. *Appl Environ Microbiol* 2001; **67**(8): 3712-5

15. M. Vleugels, G. Shama, X.T.Deng, E.Greenacre, T. Brocklehurst, M.G. Kong. Atmospheric plasma inactivation of biofilm-forming bacteria for food safety control. *IEEE Trans. Plasma Sci.,* 2005; **33**: 824-828

16. E. Kujundzic, D.A. Zander, M. Hernandez, L.T. Angenent, D.E. Henderson, S.L. Miller. Effects of ceiling-mounted HEPA-UV air filters on airborne bacteria concentrations in an indoor therapy pool building. *J Air Waste Manag Assoc* 2005; **55**(2): 210-218

17. A. Pal, S.O. Pehkonen, L.E. Yu, M.B. Ray. Photocatalytic Inactivation of Airborne Bacteria in a Continuous-Flow Reactor. *Ind Eng Chem Res* 2008; **47** (20): 7580-7585

18. A. Pal , X. Min, L.E Yu, S.O. Pehkonen, M.B. Ray. Photocatalytic Inactivation of Bioaerosols by TiO2 Coated Membrane. *Int. J. Chem. Reactor Eng.*2005; **3**: 1

19. A. Pal, S.O. Pehkonen, L.E. Yu, M.B. Ray. Photocatalytic inactivation of Gram-positive and Gram-negative bacteria using fluorescent light. *J Photoch Photobio A* 2007; **186**: 335-341

20. W.J. Kowalski, W.P. Bahnfleth, T.S. Whittam. Bactericidal effects of high airborne ozone concentrations on *Escherichia coli* and *Staphylococcus* aureus. *Ozone Sci. Eng.* 1998; **20**: 205-221

21. M G Kong, G Kroesen, G Morfill, T Nosenko, T Shimizu, J van Dijk, J L Zimmermann. Plasma medicine: an introductory review. *New J. Phys.* 2009; **11**: 115012

22. M.J. Gallagher, N. Vaze, S. Gangoli, V.N. Vasilets, A.F. Gutsol, T.N. Milovanova, S. Anandan, D.M. Murasko, A.A. Fridman. Rapid Inactivation of Airborne Bacteria Using Atmospheric Pressure Dielectric Barrier Grating Discharge. *IEEE Transactions on Plasma Science.* 2007 ; **35(5)**: 1501 - 1510

23. N.D. Vaze, K.P. Arjunan, Michael J. Gallagher, V.N. Vasilets, A. Gutsol, A. Fridman, S. Anandan. Air and Water Sterilization using Non-Thermal Plasma. *, 2007. ICOPS 2007. IEEE 34th International Conference on Plasma Science*, DOI: 10.1109/PPPS.2007.4346053 : 2007 , Page(s): 747

24. N. Vaze, S. Park, G. Fridman, A. Fridman, Direct exposure to a single filament of DBD plasma leads to the inactivation of airborne bacteria. *2010 Abstracts IEEE International Conference on Plasma Science.* DOI: 10.1109/PLASMA.2010.5533905 Publication Year: 2010 , Page(s): 1

25.Y. Liang, Y.Wu, K. Sun, Q. Chen, F. Shen, J. Zhang, M. Yao, T. Zhu, J. Fang. Rapid Inactivation of Biological Species in the Air using Atmospheric Pressure Nonthermal Plasma. *Environ. Sci. Technol.*, 2012; **46 (6)**: 3360–3368

26. K.G. Tirsell, V.P. Karpenko. A General Purpose Sub-kev X-ray Facility at the Stanford Synchrotron Radiation Laboratory. *Nucl Instrum Methods Phys Res Sect A* 1990; **291**: 511–517.

27. R. Vyhnalkova, A. Eisenberg, T.G.M. van de Ven. Deactivation Efficiency of Stabilized Bactericidal Emulsions. *Langmuir* 2011; **27**(18): 11296–11305

28. J. Ren, W.Z. Wang, L. Zhang, J. Chang, S. Hu. Photocatalytic inactivation of bacteria by photocatalyst Bi2WO6 under visible light. *Catal. Commun.*2009; **10**: 1940−1943

29. H.M. Al-Qadiri, M.A. Al-Holy, M. Lin, N.I. Alami, A.G. Cavinato, B.A. Rasco. Rapid Detection and Identification of *Pseudomonas aeruginosa* and *Escherichia coli* as Pure and Mixed Cultures in Bottled Drinking Water Using Fourier Transform Infrared Spectroscopy and Multivariate Analysis. *J. Agric. Food Chem* 2006; **54** (16): 5749-5754

30. J. Schmitt, H.C. Flemming. FTIR-spectroscopy in microbial and material analysis. *Int. Biodeterior. Biodegrad.*1998; **41** (1): 1-11.

31. M. Kansiz, P. Heraud, B. Wood, F. Burden, J. Beardall, D. McNaughton. Fourier transform infrared microspectroscopy and chemometrics as a tool for the discrimination of cyanobacterial strains. *Phytochemistry* 1999; **52** (3): 407-417.

32. L.P. Choo-Smith, K. Maquelin, T.V. Vreeswijk *et al*. Investigating microbial (micro) colony heterogeneity by vibrational spectroscopy. *Appl. Environ. Microbiol* 2001; **67** (4): 1461-1469.

33. M. Lin, M. Al-Holy, H. Al-Qadiri *et al*. Discrimination of intact and injured *Listeria monocytogenes* by Fourier transform infrared spectroscopy and principal component analysis. *J. Agric. Food. Chem.* 2004; **52**: 5769-5772

34. J.J. Ojeda, M.E. Romero-Gonzalez, R.T. Bachmann, R.G.J. Edyvean, S.A. Banwart. Characterization of the Cell Surface and Cell Wall Chemistry of Drinking Water Bacteria by Combining XPS, FTIR Spectroscopy, Modeling, and Potentiometric Titrations. *Langmuir* 2008; **24**: 4032-4040

35. G. Vedantham, H.G. Sparks, S.U. Sane, S. Tzannis, T.M. Przybycien. A holistic approach for protein secondary structure estimation from infrared spectra in H(2)O solutions. *Anal. Biochem.* 2000; **285**: 33-49

36. J. Kiwi, V. Nadtochenko. Evidence for the Mechanism of Photocatalytic Degradation of the Bacterial Wall Membrane at the TiO2 Interface by ATR-FTIR and Laser Kinetic Spectroscopy. *Langmuir* 2005; **21** (10): 4631-4641

37. A.R. Badireddy, B.R. Korpol, S. Chellam *et al*. Spectroscopic Characterization of Extracellular Polymeric Substances from *Escherichia coli* and *Serratia marcescens*: Suppression Using Sub-Inhibitory Concentrations of Bismuth Thiols. *Biomacromolecules* 2008; **9** (11): 3079–3089

38. V. Guine, L. Spadini, G. Sarret *et al*. Zinc sorption to three gram-negative bacteria: Combined titration, modeling and EXAFS study. *Environ. Sci. Technol.* 2006; **40**: 1806-1813.

39. W. Jiang, A. Saxena, B. Song, B.B. Ward, T.J. Beveridge, S.C.B Myneni. Elucidation of functional groups on gram-positive and gram-negative bacterial surfaces using infrared spectroscopy. *Langmuir* 2004; **20**: 11433-11442.

40. A. R. Badireddy, B. R. Korpol, S. Chellam, P. L. Gassman, M. H. Engelhard, A. S. Lea, and K. M. Rosso. Spectroscopic Characterization of Extracellular Polymeric Substances from *Escherichia coli* and *Serratia marcescens*: Suppression Using Sub-Inhibitory Concentrations of Bismuth Thiols. *Biomacromolecules* 2008, **9***,* 3079–3089

41.K. M. R. Kallury, M. Thompson, C. P. Tripp and M. L. Hair. Interaction of Silicon Surfaces Silanized with Octadecylchlorosilanes with Octadecanoic Acid and Octadecanamine Studied by Ellipsometry, X-ray Photoelectron Spectroscopy, and Reflectance Fourier Transform Infrared Spectroscopy. *Langmuir* 1992,**8**, 947-954

42.K. Bierbaum, M. Kinzler, Ch. Woll, M. Grunze, G. Hahner, *S.* Heid and F. Effenberger. A Near Edge X-ray Absorption Fine Structure Spectroscopy and X-ray Photoelectron Spectroscopy Study of the Film Properties of Self-Assembled Monolayers of Organosilanes on Oxidized Si( 100) A Near Edge X-ray Absorption Fine Structure Spectroscopy and X-ray Photoelectron Spectroscopy Study of the Film Properties of Self-Assembled Monolayers of Organosilanes on Oxidized Si( 100). *Langmuir* 1995,**11***,* 512-518

43.K. Syres, A. Thomas, F. Bondino, M. Malvestuto, and M. Grätzel. Dopamine Adsorption on Anatase $TiO_2$(101): A Photoemission and NEXAFS Spectroscopy Study. *Langmuir* 2010, **26**, 14548–14555

44. K.H. Schleifer, O. Kandler. Peptidoglycan types of bacterial cell walls and their taxonomic implications. *Bacteriology Reviews* 1972; **36** (4): 407- 477

45. R. Benz, K. Bauer. Permeation of hydrophilic molecules through the outer membrane of gram-negative bacteria. *Eur. J. Biochem.*1988; **16**: 1-19

46. A. Brooks, J. Yau, S. Pham. Stringent Response Changes Cell Membrane Permeability in *Escherichia coli* but does not Develop Cross Tolerance to Kanamycin, Tetracycline and Ampicillin. *Journal of Experimental Microbiology and Immunology* 2011; **15**: 30 – 35

47. R.E. Hancock. The bacterial outer membrane as a drug barrier. *Trends Microbiol* 1997; **5** (1): 37-42

48. T. Nakae, J. Ishii, M. Tokunaga. Subunit structure of functional porin oligomers that form permeability channels in the outer membrane of Escherichia coli. *J Biol Chem* 1979; **254** (5): 1457-1461

49. H. Nikaido. Prevention of drug access to bacterial targets - permeability barriers and active efflux. *Science* 1994; **264**: 382-388

50. W. Wang, Y. Yu, T. An. Visible-Light-Driven Photocatalytic Inactivation of *E.coli* K-12 by Bismuth Vanadate Nanotubes: Bactericidal Performance and Mechanism. *Environ. Sci. Technol.* 2012; **46** (8): 4599-4606

51. P. Wua, J.A. Imlay, J.K. Shang. Mechanisms of Escherichia coli inactivation on palladium-modified nitrogen-doped titanium oxide. *Biomaterials* 2010; **31**(29): 7526-7533

52. H.Yang, X. Li, Q. Zhao, G. Chen, C.L. Raston. Role of Hydroxyl Radicals and Mechanism of *Escherichia coli*. Inactivation on Ag/AgBr/TiO2 Nanotube Array Electrode under Visible Light Irradiation. *Environ. Sci. Technol.* 2012; **46** (7): 4042−4050

53. P.G. Wu, J.A. Imlay, J.K. Shang. Mechanism of *Escherichia coli* inactivation on palladium-modified nitrogen-doped titanium dioxide. *Biomaterials* 2010; **31** (29): 7526−7533.

54. K. Ishizaki, K. Sawadaishi, K. Miura, N. Shinriki. Effect of ozone on plasmid DNA of Escherichia coli in situ. *Water Research* 1987; **21**(7): 823-828

## Figures

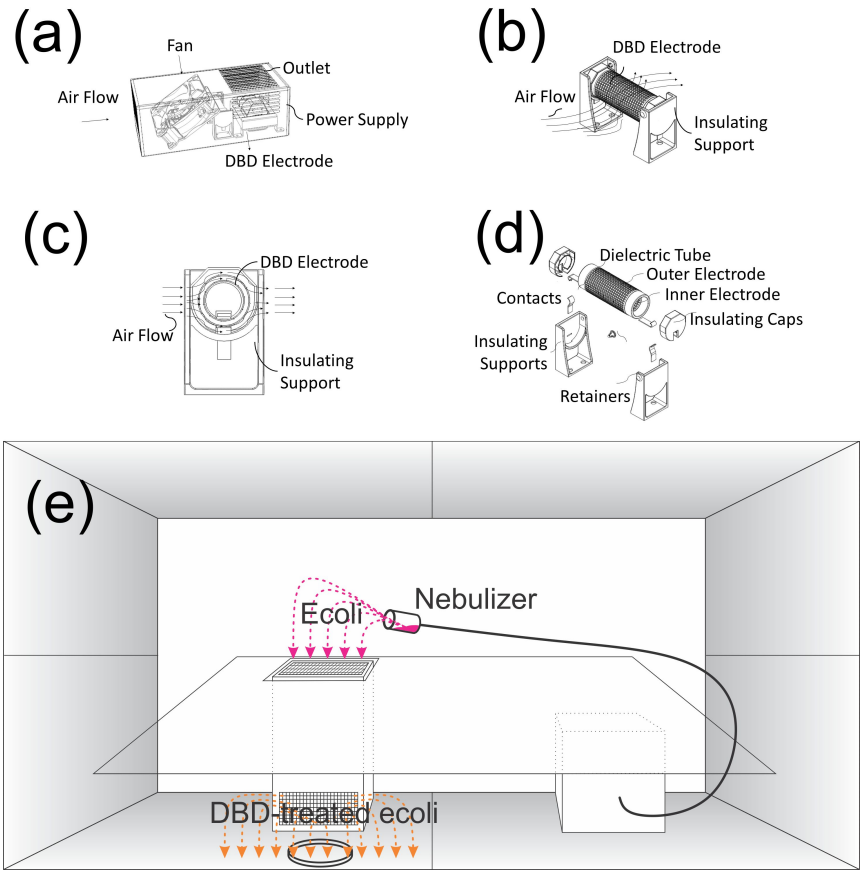


**Figure 1**

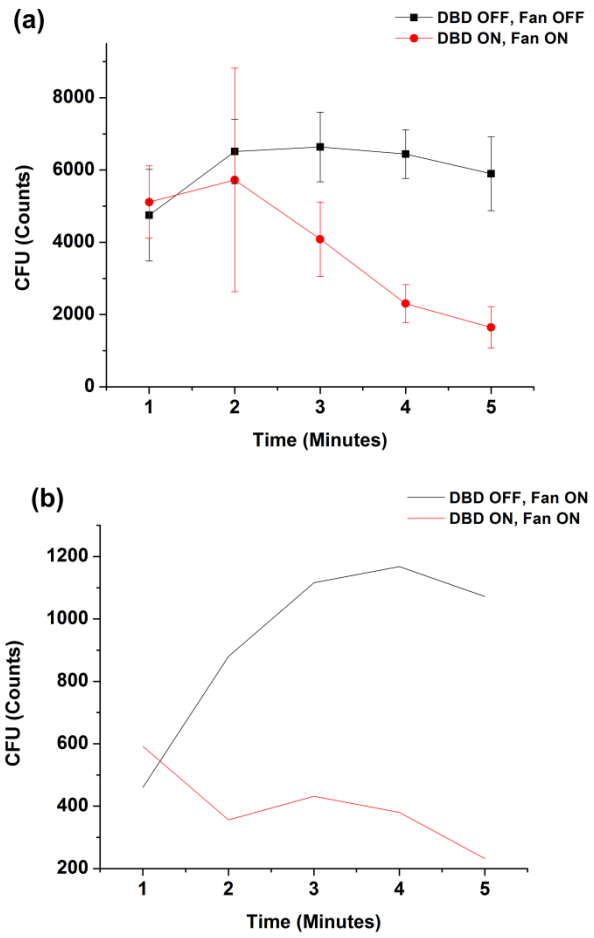
(a)
DBD OFF, Fan OFF
DBD ON, Fan ON
CFU (Counts)
0
2000
4000
6000
8000
1
2
3
4
5
Time (Minutes)
(b)
DBD OFF, Fan ON
DBD ON, Fan ON
CFU (Counts)
200
400
600
800
1000
1200
1
2
3
4
5
Time (Minutes)

**Figure 2**

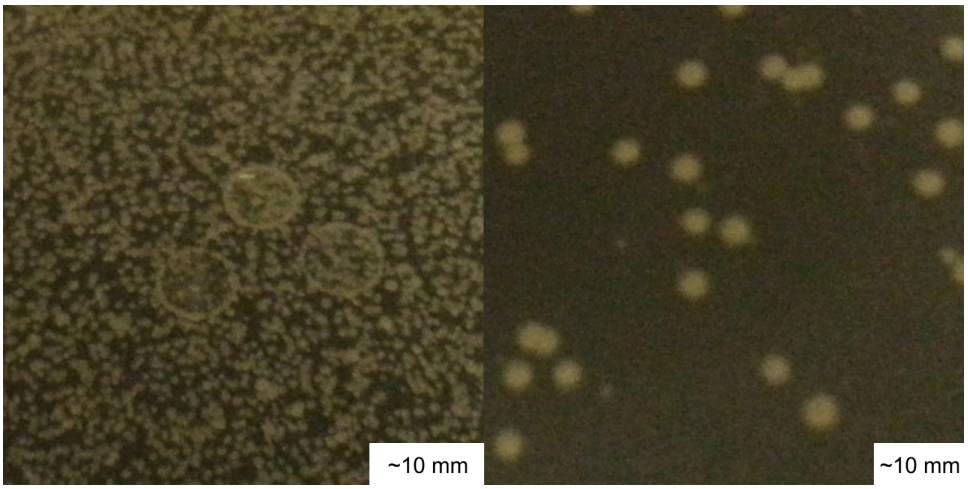


**Figure 3**

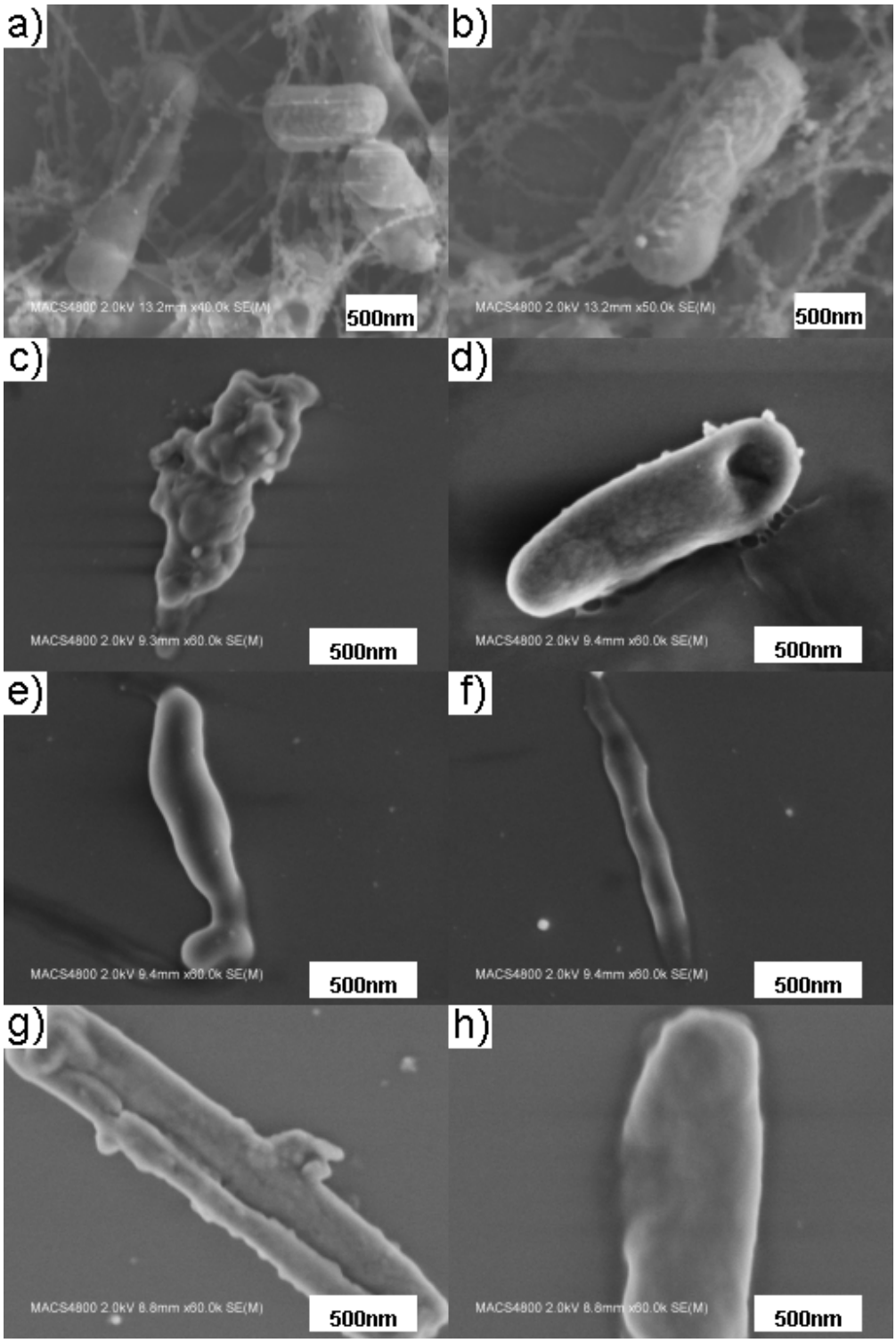
a)
MACS4800 2.0kV 13.2mm x40.0k SE(M)
500nm
b)
MACS4800 2.0kV 13.2mm x50.0k SE(M)
500nm
c)
MACS4800 2.0kV 9.3mm x60.0k SE(M)
500nm
d)
MACS4800 2.0kV 9.4mm x60.0k SE(M)
500nm
e)
MACS4800 2.0kV 9.4mm x60.0k SE(M)
500nm
f)
MACS4800 2.0kV 9.4mm x60.0k SE(M)
500nm
g)
MACS4800 2.0kV 8.8mm x60.0k SE(M)
500nm
h)
MACS4800 2.0kV 8.8mm x60.0k SE(M)
500nm

**Figure 4**

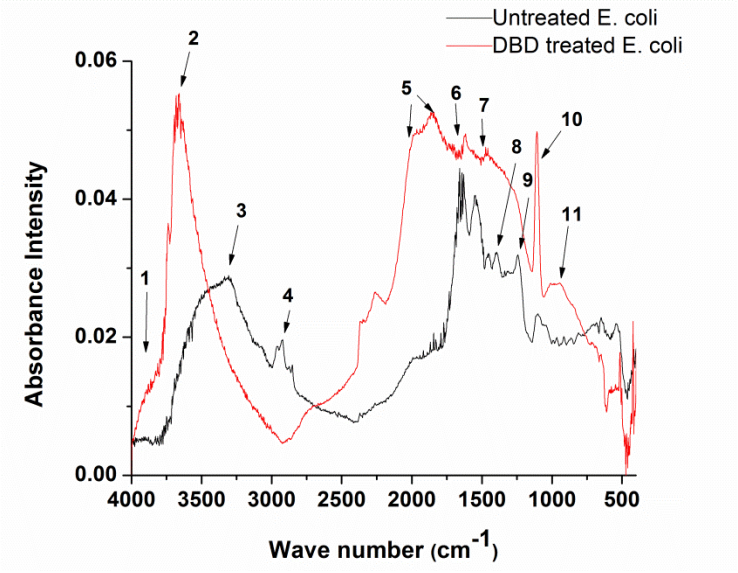
Untreated E. coli
DBD treated E. coli
Absorbance Intensity
0.06
0.04
0.02
0.00
4000
3500
3000
2500
2000
1500
1000
500
Wave number (cm-1)
1
2
3
4
5
6
7
8
9
10
11

**Figure 5**

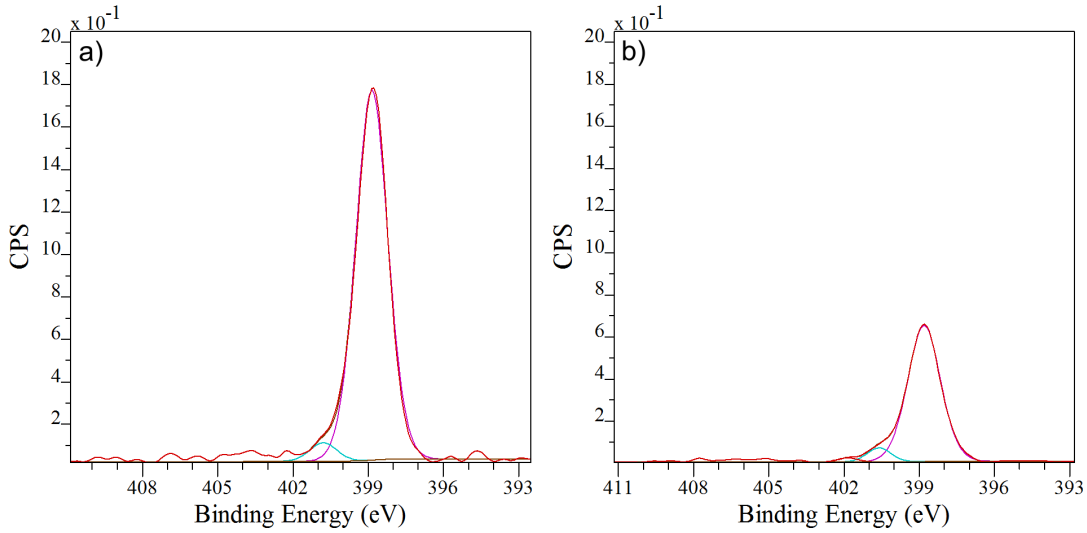
a)
b)
x 10-1
CPS
Binding Energy (eV)
20
18
16
14
12
10
8
6
4
2
408
405
402
399
396
393
411

**Figure 6**

**Figure captions**

**Figure 1.** (a) Schematic of the NV200 DBD system, (b) diagram of the assembled coil, (c) cross section illustrating the air flow around the dielectric barrier discharge, (d) the coil parts, and (e ) the experimental setup for inactivation E. coli and sample collection

**Figure 2.** E. coli counts captured from air in an agar plate and re-cultured. (a) both DBD and fan ON, control experiment with both DBD and fan OFF in 100 mm diameter agar plate, (b) DBD and fan ON, Control experiment with DBD OFF and Fan ON in 60 mm diameter agar plate.

**Figure 3.** Photograph of the E. coli captured from air and re-cultured in a 100 mm diameter petri dish containing tryptic soy agar (left) control experiment with DBD OFF (right) DBD ON

**Figure 4.** Scanning electron microscopic image of (a,b) untreated E.coli and (c-h) E. coli passed through the DBD and captured from air

**Figure 5.** FTIR spectroscopy analysis of untreated and DBD-treated E. coli. Peak attribution: 1, 2 - OH functionalities due to oxidation of hydrocarbons, 3, 6- Vibrations of Amine functionalities (amine and amide), 4: alkyl CH2 and CH3 vibrations, 5: unknown, 7,8: CH vibration, 9: Phosphate groups present in cell membrane, 10: P=O, C-O-C, C-O-P, 11: OH functionality.

**Figure 6.** N 1s Core level x ray photoemission spectrum (XPS) of (left) untreated E. coli and (right) inactivated E. coli